

## Article

# Numerical Simulation of the Smoke Distribution Characteristics in a T-Shaped Roadway

Cui Ding <sup>1,2,\*</sup>, Dou Chang <sup>2</sup>, Diange Sun <sup>2</sup> and Songling Zou <sup>2</sup>

<sup>1</sup> State Key Laboratory Cultivation Base for Gas Geology and Gas Control, Henan Polytechnic University, Jiaozuo 454000, China

<sup>2</sup> School of Safety Engineering, China University of Labor Relations, Beijing 100048, China; changdou@culr.edu.cn (D.C.); sundiange@aliyun.com (D.S.); 2090805012@stu.culr.edu.cn (S.Z.)

\* Correspondence: dingcui@culr.edu.cn

**Abstract:** This paper numerically analyzes the influence of heat release rate (HRR) and longitudinal ventilation velocity on smoke distribution characteristics in a T-shaped roadway when the fire source was located upstream of the T-junction. The back-layering length, critical ventilation velocity, smoke temperature, and CO concentration in the main and branched roadway were investigated and analyzed. The results showed that the ventilation velocity is the key factor influencing back-layering length, while the effect of HRR on back-layering length is gradually weakened as HRR increases. The critical ventilation velocity in the T-shaped roadway is higher than in a single-tube roadway, and the predicted model of dimensional critical ventilation velocity in a T-shaped bifurcated roadway is proposed. The correlation between average temperature ( $Z = 1.6$  m) (both in the main roadway I and the branched roadway) and ventilation velocity fits the power function, and the variation in average temperature ( $Z = 1.6$  m) according to HRR fits the linear formula. The relation between average concentration of CO ( $Z = 1.6$  m) (both inside the main roadway I and the branched roadway) and longitudinal ventilation velocity follows the power relation, and the variation in average concentration of CO ( $Z = 1.6$  m) according to HRR follows the linear function.

**Keywords:** mine fire; bifurcated roadway; CFD; critical velocity; smoke distribution



**Citation:** Ding, C.; Chang, D.; Sun, D.; Zou, S. Numerical Simulation of the Smoke Distribution Characteristics in a T-Shaped Roadway. *Fire* **2024**, *7*, 80. <https://doi.org/10.3390/fire7030080>

Academic Editors: Yanming Ding, Kazui Fukumoto and Jiaqing Zhang

Received: 9 January 2024

Revised: 23 February 2024

Accepted: 24 February 2024

Published: 3 March 2024



**Copyright:** © 2024 by the authors. Licensee MDPI, Basel, Switzerland. This article is an open access article distributed under the terms and conditions of the Creative Commons Attribution (CC BY) license (<https://creativecommons.org/licenses/by/4.0/>).

## 1. Introduction

The underground roadway of mines is a confined space; once fire occurs in the roadway, the high-temperature smoke generates fire pressure and a throttling effect, which can lead to airflow disorder. And the high-temperature smoke will propagate rapidly in the roadway, which will reduce the escape space and threaten workers' lives and health [1–4]. The T-shaped roadway is commonly used in mines; due to the complex geometric characteristics of the T-shaped structure, the fire dynamics and smoke spread in bifurcated roadways will be more complex than in straight roadways.

The smoke distribution in bifurcated roadways and bifurcated tunnels has been studied extensively by many scholars. Xue [5] researched the effect of the bifurcated angle of inclined roadways on the velocity distribution and smoke temperature by using pyrosim software. Lu et al. [6] studied the influence of ambient temperature, ventilation velocity, and heat release rate on smoke temperature and visibility in T-shaped roadways by the numerical simulation method. Gao et al. [7] conducted a series of small-scale fire experiments, measured the back-layering length and smoke temperature in bifurcated tunnels, and proposed the temperature decay model in the main tunnel and the branched tunnel.

Huang et al. [8,9] experimentally investigated thermal smoke movement in branched tunnels, established the predicted model of the maximum ceiling temperature, and quantified the smoke back-layering length under different heat release rates and various longitudinal ventilation velocities. The empirical model is proposed to predict the smoke

back-layering length in branched tunnels. Chen et al. [10] compared the smoke temperature distribution of single-line tunnels with T-shaped tunnels by experimentation and developed the modified double-exponential correlation to describe the longitudinal temperature decay process in the entire spreading region of fire smoke in T-shaped tunnel fires. Tao et al. [11] established a model tunnel to research the impact of fire location, bifurcated shaft exhaust velocity, and longitudinal velocity on ceiling temperature and they proposed the temperature decay model. Some scholars [12–19] conducted a series of experiments to study the critical velocity and the smoke backflow in single-line tunnel fires and proposed the prediction model of the dimensionless back-layering length and the ratio of ventilation velocity to critical velocity. Gannouni et al. [20,21] investigated the effect of obstacles on the back-layering length and the critical velocity in single-line tunnel fires by using Fire Dynamic Simulator (FDS) and developed the model to calculate the back-layering arrival time. Lu et al. [22] researched the longitudinal temperature distribution and maximum ceiling temperature by experimentation and the simulation method and proposed a mathematical model to predict the maximum rise in ceiling temperature and the longitudinal temperature distribution in the bifurcated tunnel. Liu et al. [23] studied the effect of longitudinal fire location on temperature distribution in bifurcated roadways and developed empirical models of the maximum temperature in the main tunnel and temperature decay in the branched tunnel.

By and large, the previous studies on bifurcation structure fires focus on tunnel fires, the decay process of ceiling temperature, the maximum rise in ceiling temperature, and the critical ventilation velocity, which were thoroughly studied in bifurcated tunnel fires. Bifurcated roadway fires have been seldom researched; in particular, the back-layering length, temperature, and CO concentration distribution in the main and branched roadways have rarely been studied. The underground space of roadways is smaller than a tunnel, so the smoke will propagate more fully and smoking control measures and emergency rescue will differ from tunnel fires.

Therefore, in order to investigate the smoke distribution characteristics in bifurcated roadways, the T-shaped roadway was selected as the roadway model; the fire source was located upstream of the T-junction, heat release rate and ventilation velocity were selected as the factors affecting the smoke diffusion, and ANSYS 18.0 was used to simulate the smoke distribution in the main roadway and branched roadway. The critical velocity and the temperature and CO concentration distribution at breathing zone height in the main roadway and the branched roadway were thoroughly analyzed in this paper in order to provide suggestions for emergency rescue and personnel evacuation during underground roadway fires.

## 2. Simulation Methods

### 2.1. Physical Model

Based on the actual underground roadway, the 3D geometric model of T-shaped roadways was established. The size of the main roadway was  $3\text{ m} \times 3\text{ m} \times 403\text{ m}$ ; the branch roadway was in the center of the main roadway and the size was  $3\text{ m} \times 3\text{ m} \times 200\text{ m}$ . All cross-sections were rectangular, with a width of 3 m and a height of 3 m. Because the upstream smoke would have been pushed into both the main roadway and branched roadway, the fire source was set upstream of the T-junction. The distance from the center of the fire source to the velocity inlet was 189 m, the length of the fire source was 2 m, and the flame height was chosen to be 3 m; these were the limitations set by the roadway roof. The cross-section of the geometric model of the T-shaped roadway and coordinate system is shown in Figure 1, and the Z-direction is the height direction of the roadway.

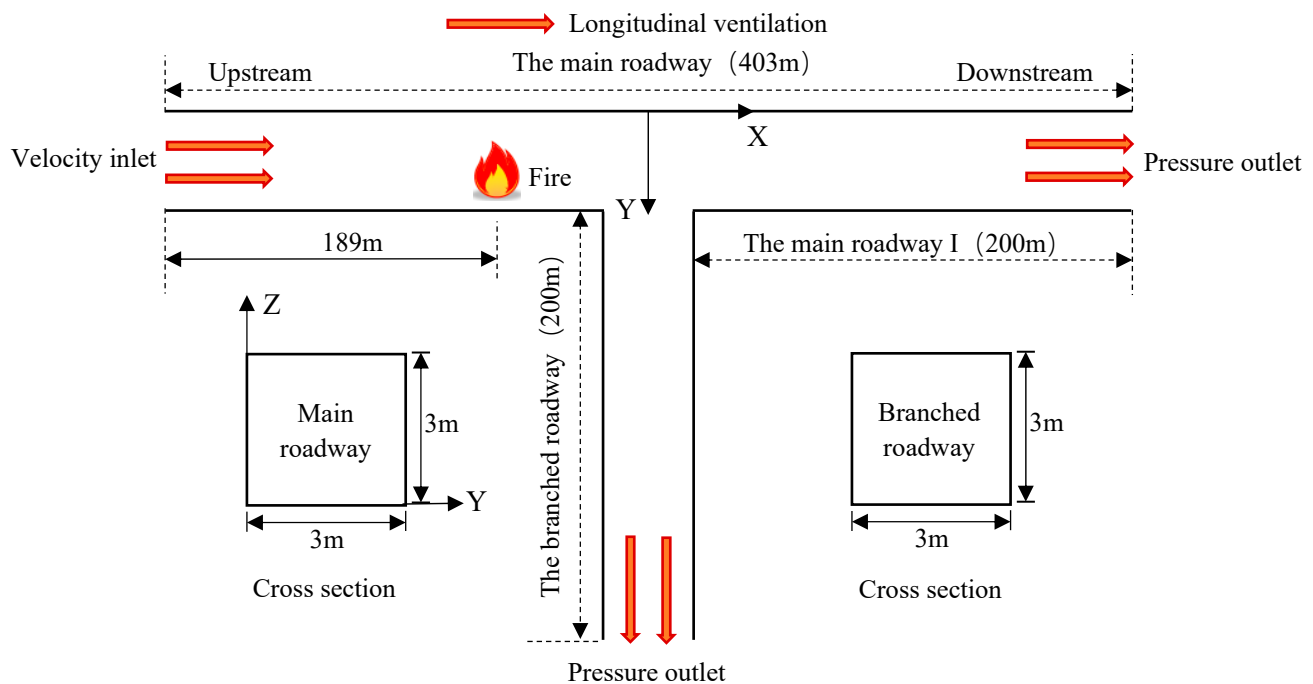


**Figure 1.** The physical model of the T-shaped roadway in cross-section.

## 2.2. Boundary Conditions and Assumptions

The standard  $k - \varepsilon$  equation and transport equation were chosen to simulate the turbulent flow of airflow and smoke diffusion [24], and the above equations have been extensively used in the fire simulation by scholars. The airflow inlet of the main roadway was set to be the velocity inlet and the airflow outlet of the main roadway and branched roadway were set to be the pressure outlet, as shown in Figure 1. The fire source was defined as the source term, and it was represented by a volumetric source. Due to the thermal radiation of the fire source, the temperature inside the roadway increases and the gas density in the T-shaped roadway would have been changed. Meanwhile, natural convection of gas in the vertical direction would be caused by gravity. So, the influence of gravity and buoyancy effect on air flow were considered in the simulation.

The following assumptions were adopted in the numerical simulation calculations: fresh airflow and fire smoke were considered incompressible fluids; there was no sliding on the roadway wall and no heat exchange between the wall and the air inside the roadway; obstacles such as mining cars and workers in the roadway were ignored; the effect of gas, dust, and blasting smoke on the airflow and smoke diffusion were not considered; the combustion process of the fire was not considered; the fire source was set as an energy source with a fixed rate of heat release [25]; the smoke generated by the fire was presented by CO; and the amount of CO generated by the fire was calculated according to Equation (1) [26]:

$$F_r = Q \times \gamma_{co} \quad (1)$$

where  $F_r$  represents the amount of CO generated by the fire ( $\text{m}^3/\text{s}$ ),  $Q$  represents the heat release rate (kW), and  $\gamma_{co}$  represents the constant of CO generation rate ( $\text{m}^3/\text{kJ}$ ) ( $3.22 \times 10^{-6} \text{ m}^3/\text{kJ}$ ) [27].

## 2.3. Parameters

In the simulation, the ambient temperature was  $25^\circ\text{C}$ , the gravitational acceleration was  $9.81 \text{ m/s}^2$ , and the ambient pressure was 101,325 Pa. The longitudinal ventilation velocities were  $1 \text{ m/s}$ – $3 \text{ m/s}$  in the main roadway, the heat release rates were 300 kW, 600 kW, 900 kW, and 1200 kW, respectively, and the total simulation cases were 35. Then, the

influence of heat release rate and ventilation velocity on smoke diffusion and distribution characteristics were analyzed and discussed; the simulation cases are shown in Table 1.

**Table 1.** The parameters and simulation cases.

Heat Release Rate/kw	Longitudinal Ventilation Velocity/(m·s <sup>-1</sup> )	Hydraulic Diameter/m
300	1, 1.1, 1.2, 1.3, 1.4, 1.5, 2, 2.5, 3	3
600	1, 1.1, 1.2, 1.3, 1.4, 1.5, 1.6, 1.7, 1.8, 1.9, 2, 2.5, 3	3
900	1, 1.1, 1.2, 1.4, 1.5, 1.6, 1.7, 1.8, 1.9, 2, 2.5, 3	3
1200	1, 1.5, 2, 2.1, 2.5, 3	3

**2.4. Mesh**

In order to validate the independence of mesh, four kinds of cell sizes were chosen to simulate the roadway fire, which are 0.15 m × 0.15 m × 0.15 m, 0.2 m × 0.2 m × 0.2 m, 0.25 m × 0.25 m × 0.25 m, and 0.28 m × 0.28 m × 0.28 m, respectively. Figure 2 shows the horizontal and vertical temperature distribution in the main roadway when the heat release rate is 600 kw and the ventilation velocity is 2 m/s. It can be seen that, when the interval sizes of the grid are 0.15 m and 0.2 m, the difference in lateral temperature distribution and in longitudinal temperature distribution are very small; so, taking into account both the computational accuracy and time cost, a cell size of 0.2 m × 0.2 m × 0.2 m is selected and the total number of cells is 678,375.

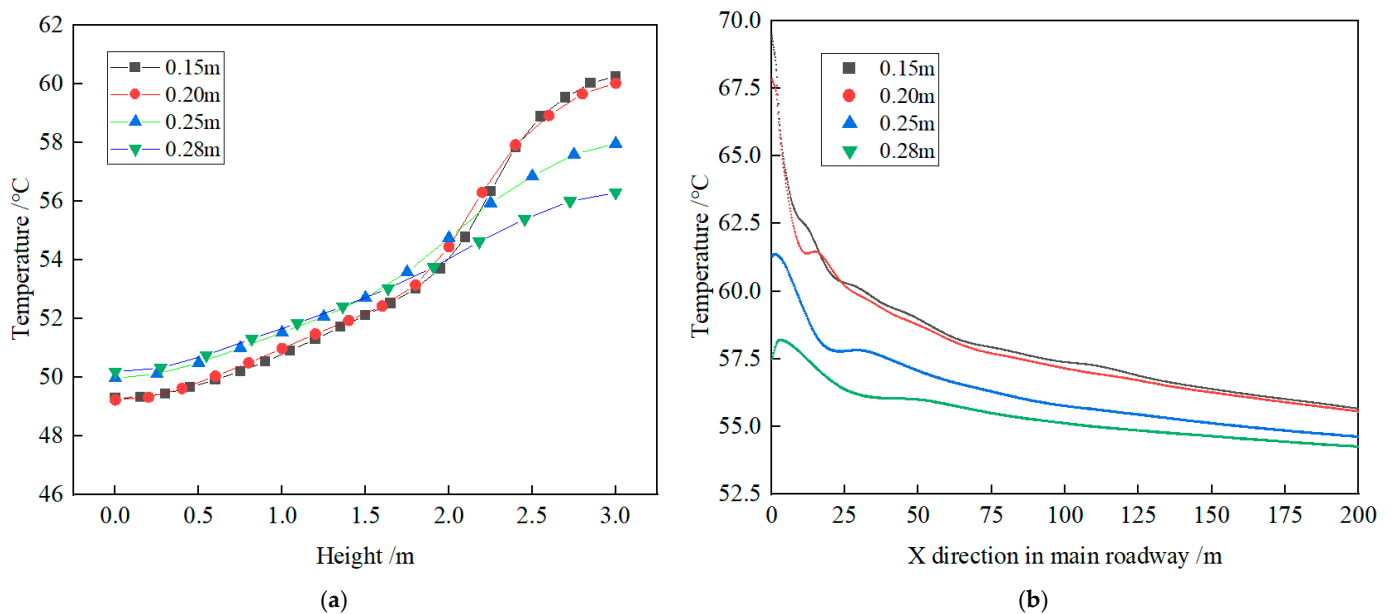


**Figure 2.** Validation of numerical method by grid independence. (a) The vertical temperature distribution at X = 30 m in the main roadway. (b) The longitudinal temperature distribution at Z = 2.9 m in the main roadway.

**3. Results and Discussion**

**3.1. Back-Layering Length and Critical Velocity**

Back-layering length is the important parameter in roadway fires. The back-layering flow is the most fatal contamination to workers who are blocked in upstream of the fire source.

Figure 3 shows the relationship between back-layering length and longitudinal ventilation velocity under different heat release rates. Figure 3 indicates that the back-layering length decreases constantly as the ventilation velocity increases and presents a linear trend. Moreover, under the same ventilation velocity, the back-layering length increases as the heat release rate increases. However, when the heat release rate is more than 600 kw, the

back-layering length increases quite slowly. This indicates that the influence of heat release rate on the back-layering length is gradually weakened as the heat release rate increases.

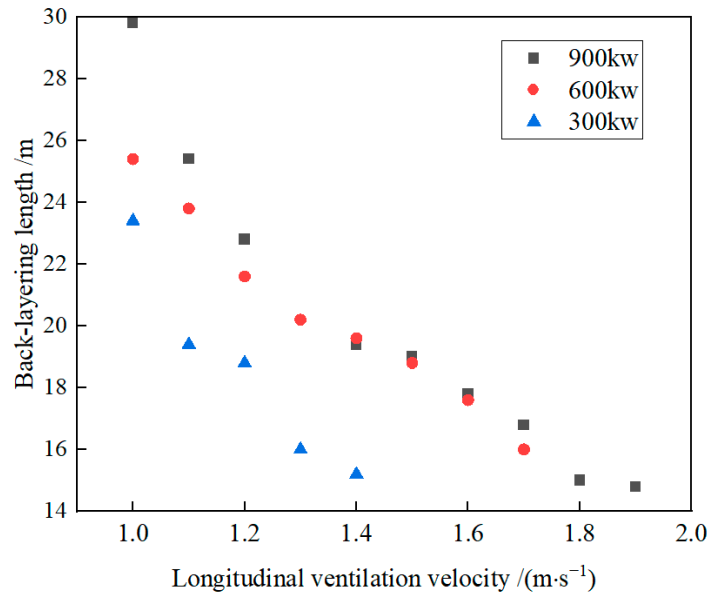


Figure 3. Relationship between back-layering length and longitudinal ventilation velocity.

Critical ventilation velocity is also a key parameter for ensuring the safety and proper emergency evacuation of workers in roadway fires. The critical ventilation velocity in single-tube tunnel fires has been researched thoroughly. Wu and Bakar [12] established a mathematical model for dimensionless critical ventilation velocity and dimensionless heat release rate in a single-tube tunnel, as shown in Equation (2):

$$v'_c = \frac{v_c}{\sqrt{gH}} = \begin{cases} 0.40[0.20]^{-1/3}[\dot{Q}]^{1/3}, & \dot{Q} \leq 0.20 \\ 0.40, & \dot{Q} > 0.20 \end{cases} \quad (2)$$

where  $v'_c$  represents the dimensionless critical ventilation velocity,  $v_c$  represents the critical ventilation velocity (m/s),  $g$  represents the gravity acceleration (m/s<sup>2</sup>),  $H$  represents the hydraulic tunnel height (m),  $\dot{Q}$  represents the dimensionless heat release rate,  $\dot{Q} = Q/\rho_0 c_p T_0 g^{1/2} H^{5/2}$ ,  $Q$  represents the heat release rate (kw),  $\rho_0$  represents the ambient air density (kg/m<sup>3</sup>),  $c_p$  represents the specific heat capacity (kJ/(kg·K)), and  $T_0$  represents the environment temperature (K).

Li et al. [13] also acquired the correlation between dimensionless critical ventilation velocity and dimensionless heat release rate in a single-tube tunnel, which can be expressed in Equation (3):

$$v'_c = \frac{v_c}{\sqrt{gH}} = \begin{cases} 0.81[\dot{Q}]^{1/3}, & \dot{Q} \leq 0.15 \\ 0.43, & \dot{Q} > 0.15 \end{cases} \quad (3)$$

where  $\dot{Q} = Q/\rho_0 c_p T_0 g^{1/2} H^{5/2}$  and  $H$  represents the tunnel height (m).

In this paper, the critical ventilation velocity was determined by the X direction velocity vector beneath the ceiling in the main roadway. The critical ventilation velocities are 1.5 m/s, 1.8 m/s, 2 m/s, and 2.1 m/s when the heat release rates (HRR) are 300 kw, 600 kw, 900 kw, and 1200 kw, respectively. The critical ventilation velocity predicted by CFD simulation under different HRRs is shown in Figure 4a, and the critical ventilation velocities calculated by equations proposed by Wu [12] and Li [13] are also presented in Figure 4a for comparison. It can be seen that the critical ventilation velocity increases with the increase in heat release rate and the increased value decreases slowly. Also, we

can find that the critical ventilation velocity is higher than Wu's and Li's model, which means the critical ventilation velocity in the T-shaped bifurcated roadway is higher than in the single-tube roadway when the fire is located upstream of the T-junction. This is because, when the airflow passes through the T-junction, a portion of ventilation mass flow is pushed into the branched roadway, so the actual ventilation mass flow in the main roadway of the T-shaped bifurcated roadway is lower than in the single-tube roadway. Figure 4b presents the correlation between dimensional critical ventilation velocity and dimensional heat release rate. According to Figure 4b,  $v'_c$  is directly proportional to  $\dot{Q}^{1/3}$ ; hence, the prediction model of dimensional critical ventilation velocity in the T-shaped bifurcated roadway can be expressed as:

$$v'_c = 0.087 + 0.75 \dot{Q}^{1/3} \quad (4)$$

It can be found that Equation (4) is similar to Equations (2) and (3) and is more close to Li's model.

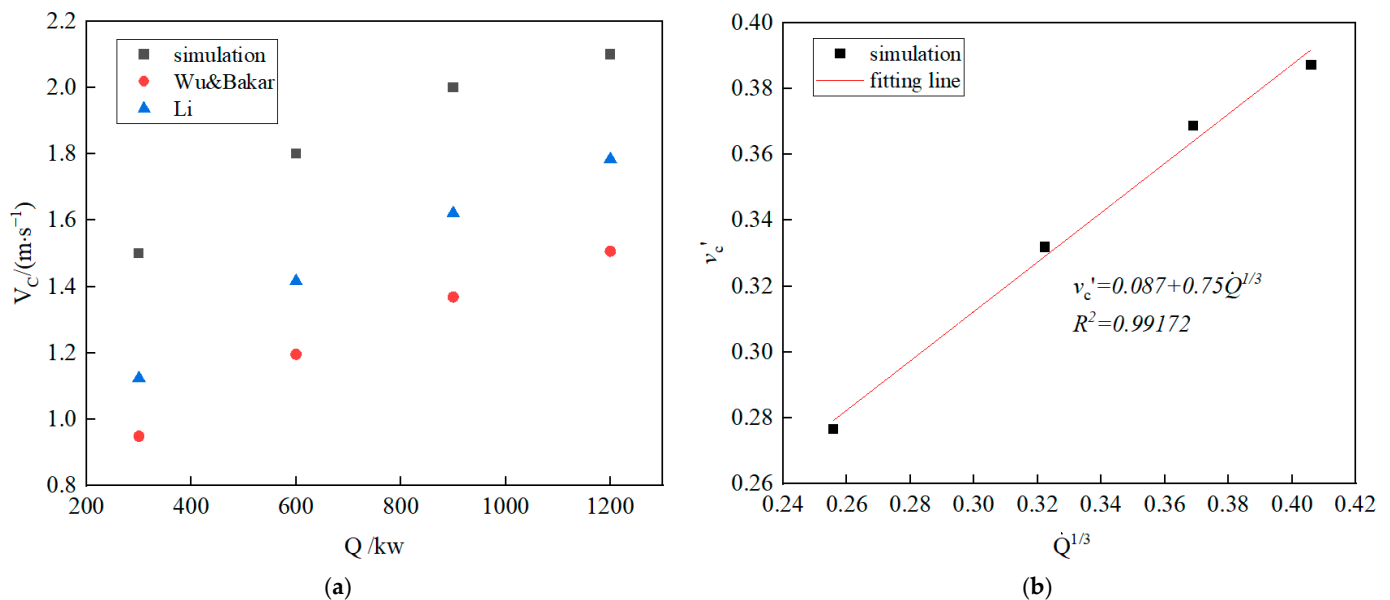


**Figure 4.** The relationship between critical ventilation velocity and heat release rate in the T-shaped bifurcated roadway. (a) Comparison between simulation and previous model; (b) the correlation between dimensional critical ventilation velocity and dimensional heat release rate.

To further validate the accuracy of the numerical model adopted in this paper, the critical ventilation velocities predicted by CFD were compared with data from Li's small-scale tests [13]. Li's small-scale experimental tests were conducted in a 12 m long model tunnel. The fire source, which was a 100 mm diameter porous bed burner, was located in the center of the tunnel model. We built the same simulated tunnel model as Li's, and the numerical model was the same as mentioned above (see Section 2.2). The fire source was set as a volumetric source with a height of 0.25 m and a diameter of 0.1 m. Table 2 presents the critical ventilation velocity predicted by CFD under different cases in Li's experiment, and the comparison between simulation values of critical ventilation velocity and tested results by Li is shown in Figure 5. According to Table 2 and Figure 5, there is a reasonable agreement between the simulation and the experiment tests.

**Table 2.** The critical ventilation velocity predicted by CFD under different cases in Li [13].

Geometric Dimensions of Tunnels	Heat Release Rate/kw	Ambient Temperature/°C	$v_c/m \cdot s^{-1}$	
			Li's Experiment	CFD
0.25 m × 0.25 m × 12 m	3.2	20	0.57	0.68
	4.8	20.8	0.63	0.7
	6.7	20.8	0.66	0.71
	9.3	23.3	0.67	0.71
	12.9	23.5	0.67	0.71
	16.7	24.5	0.67	0.71

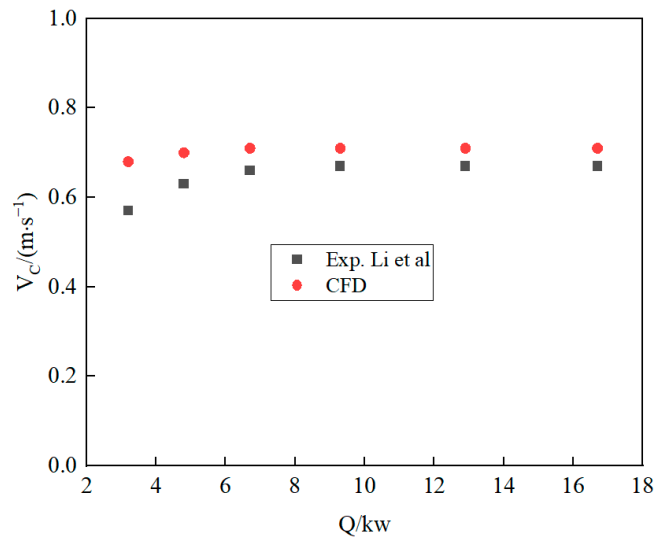


**Figure 5.** Comparison of critical ventilation velocity predicted with data from Li’s experiments [13].

### 3.2. Longitudinal Temperature Profile in the Main and Branched Roadway

Inhaling high-temperature smoke is the main factor to cause casualties in fire accidents, so the temperature distribution at breathing zone height ( $Z = 1.6$  m) was analyzed in this paper. The tolerance time in a fire environment is 12 min for a person [28], so the escape temperature that a person can escape from the fire environment successfully is set to be  $60$  °C.

Figure 6 presents the longitudinal temperature profile at breathing zone height of the main roadway when heat release rates are 300 kw, 600 kw, and 900 kw, respectively. Figure 6a illustrates that, when the longitudinal ventilation velocity is 1 m/s, the maximum temperature is located at the fire source and the value is  $101.636$  °C, and the influence range of the fire source on upstream temperature is 21.4 m, which can be explained by smoke backflow and thermal convection. When the longitudinal ventilation velocities are 1.5 m/s, 2 m/s, 2.5 m/s, and 3 m/s, respectively, the influence range of fire source on upstream temperature is 0 m and the smoke temperature at the fire source increases dramatically from  $25$  °C to  $41.16$  °C,  $37.13$  °C,  $34.73$  °C, and  $33.07$  °C, respectively; then, the temperature rises slightly and becomes steady along the longitudinal direction (X direction). The smoke temperatures in the main roadway I are all lower than escape temperature when the ventilation velocities are 1 m/s~3 m/s. As shown in Figure 6b, when the longitudinal ventilation velocities are 1 m/s and 1.5 m/s, the values of maximum temperature are  $179$  °C and  $140$  °C, respectively, and the influence ranges of fire source on upstream temperature are 24.2 m and 14 m, respectively. When the longitudinal ventilation velocities are 2 m/s, 2.5 m/s, and 3 m/s, respectively, the smoke temperature at the fire source increase dramatically from  $25$  °C to  $37.366$  °C,  $34.869$  °C, and  $33.2$  °C, respectively; then, the temperature rises slightly and becomes steady along the longitudinal direction (X direction). The smoke temperatures in the main roadway I are all lower than escape

temperature when the ventilation velocities are 2 m/s, 2.5 m/s, and 3 m/s. According to Figure 6c, when the longitudinal ventilation velocities are 1 m/s and 1.5 m/s, the values of maximum temperature are 296.96 °C and 138.8 °C, respectively, and the influence ranges of fire source on upstream temperature are 27 m and 18 m, respectively. When the longitudinal ventilation velocities are 2 m/s, 2.5 m/s, and 3 m/s, respectively, the smoke temperature at the fire source increase dramatically from 25 °C to 61.90 °C, 54.35 °C, and 49.68 °C, respectively; then, the temperature rises slightly and becomes steady along the longitudinal direction (X direction). The smoke temperatures in the main roadway I are all lower than escape temperature when the ventilation velocities are 2.5 m/s and 3 m/s.

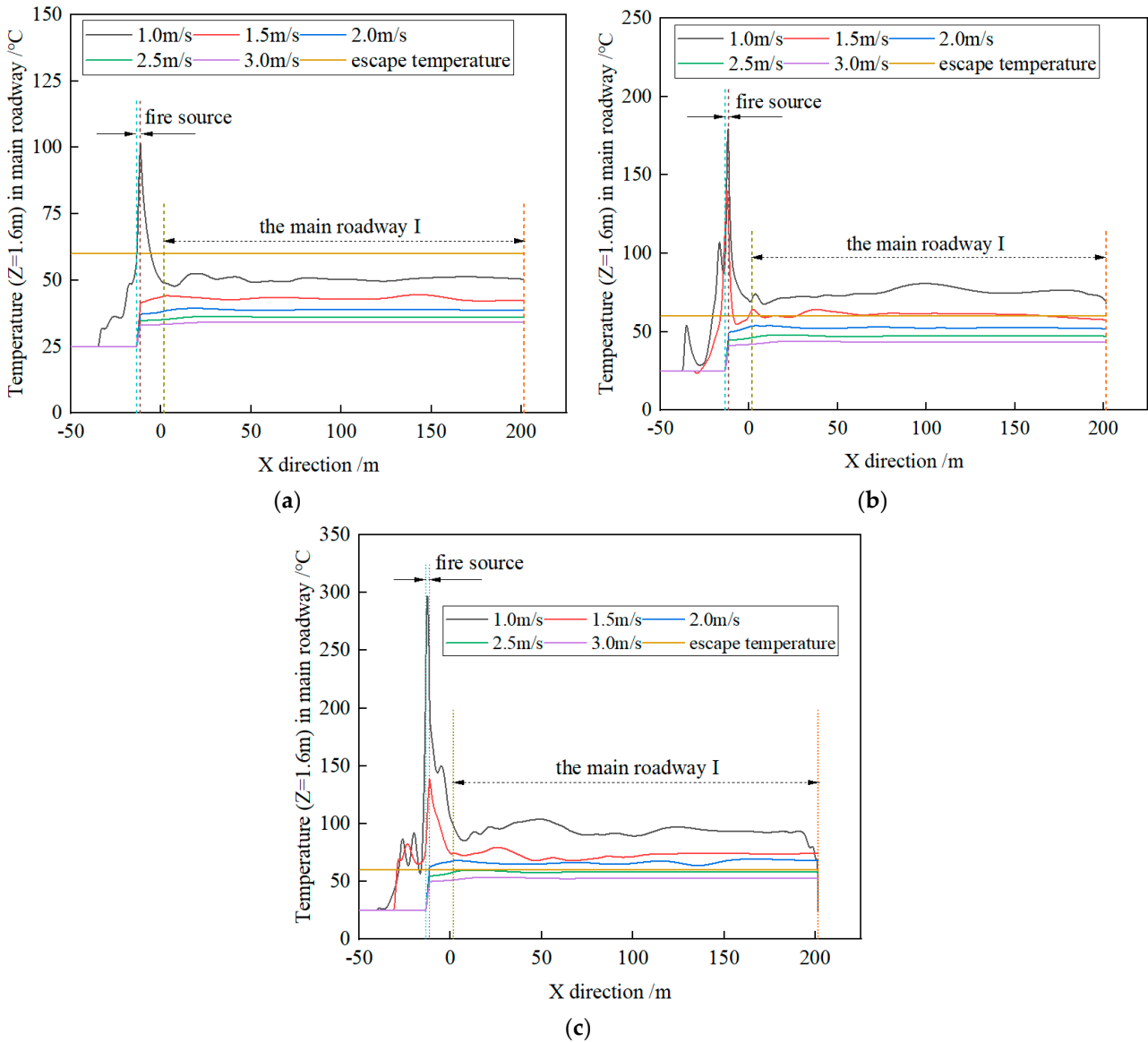


**Figure 6.** The temperature profile ( $Z = 1.6$  m) in the main roadway under different ventilation velocities and different heat release rates: (a) 300 kw; (b) 600 kw; (c) 900 kw.

Then, the effect of longitudinal ventilation velocity and heat release rate on average temperature at breathing zone height inside the bifurcated roadway is discussed thoroughly. Figure 7 presents the average temperature at  $Z = 1.6$  m inside the main roadway I and branched roadway under different ventilation velocities and different heat release rates.

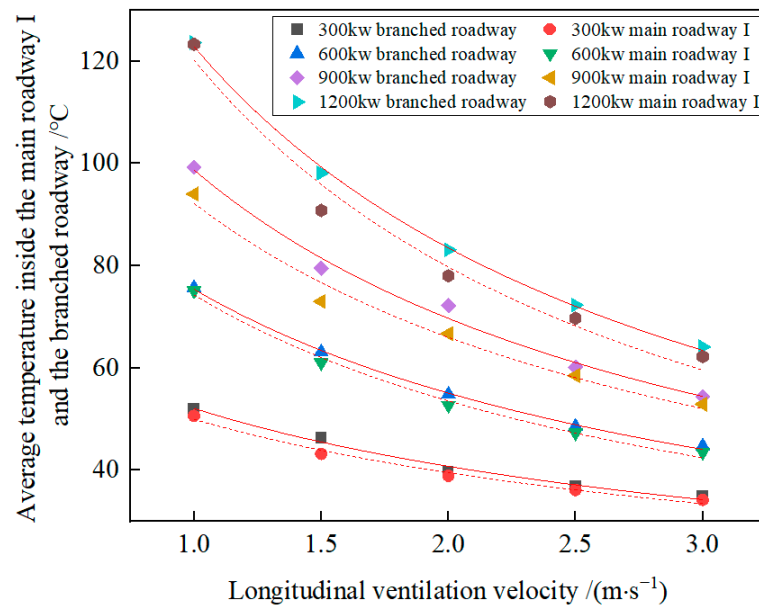


**Figure 7.** The average temperature ( $Z = 1.6$  m) inside the main roadway I and branched roadway under different ventilation velocities and different heat release rates.

It can be observed from Figure 7 that the average temperatures in the main roadway I and branched roadway are lower than  $60\text{ }^{\circ}\text{C}$  when the HRR is 300 kw and the ventilation velocities are 1 m/s, 1.5 m/s, 2 m/s, 2.5 m/s, and 3 m/s and when the HRR is 600 kw and the ventilation velocities are 2 m/s, 2.5 m/s, and 3 m/s and when the HRR is 900 kw and the ventilation velocities are 2.5 m/s and 3 m/s. The average temperatures in the branched roadway under different cases are all slightly lower than that in the main roadway I. When the heat release rate is 300 kw, the maximum temperature difference between the main roadway I and the branched roadway is  $3.1\text{ }^{\circ}\text{C}$  and the minimum temperature difference is  $0.7\text{ }^{\circ}\text{C}$ . When the heat release rate is 600 kw, the maximum temperature difference is  $2.12\text{ }^{\circ}\text{C}$  and the minimum temperature difference is  $0.585\text{ }^{\circ}\text{C}$ . When the heat release rate is 900 kw, the maximum temperature difference is  $6.47\text{ }^{\circ}\text{C}$  and the minimum temperature difference is  $1.43\text{ }^{\circ}\text{C}$ . When the heat release rate is 1200 kw, the maximum temperature difference is  $8\text{ }^{\circ}\text{C}$  and the minimum temperature difference is  $0.3\text{ }^{\circ}\text{C}$ .

Figure 7 also shows that, under different heat release rates, the average temperatures in the main roadway I and branched roadway decrease as the ventilation velocity increases. This occurs because the thermal convection between airflow and smoke is intensified with the increase in ventilation velocity. And the temperature decay fits the power function, as shown in Equation (5):

$$T = a(1 + v)^{-b} \tag{5}$$

where  $T$  represents the average temperature at  $Z = 1.6$  m ( $^{\circ}\text{C}$ ),  $v$  represents longitudinal ventilation velocity (m/s), and  $a$  and  $b$  represent dimensionless coefficient, respectively.

The fitting curves are shown with solid lines and dashed lines in Figure 7. The values of  $a$  and  $b$  are displayed in Table 3. It can be seen from Figure 7 and Table 3 the values of R-squares are all above 0.98; it can be concluded that the variation in average temperature in the main roadway I and branched roadway according to ventilation velocity can be accurately describe by Equation (5).

The variation in average temperature with the increasing heat release rate in the bifurcated roadway is shown in Figure 8. It can be observed that the average temperatures in the main roadway I and branched roadway increase constantly as the heat release rate increases, and the predicted data of average temperature can be correlated to HRR with the following equation:

$$T = c + dQ \tag{6}$$

where  $T$  represents the average temperature at  $Z = 1.6$  m ( $^{\circ}\text{C}$ ),  $Q$  represents the heat release rate (kw), and  $c$  and  $d$  represent the dimensionless coefficient, respectively.

**Table 3.** The values of coefficients  $a$  and  $b$ .

The Type of Roadway	Heat Release Rate/kw	$a$	$b$	$R^2$
the main roadway I	300	74.659	0.579	0.9892
	600	130	0.808	0.99437
	900	163.280	0.825	0.98
	1200	242.607	1.013	0.97933
the branched roadway	300	79.253	0.606	0.98865
	600	128.951	0.774	0.99875
	900	179.1	0.859	0.99
	1200	237.95	0.954	0.9988

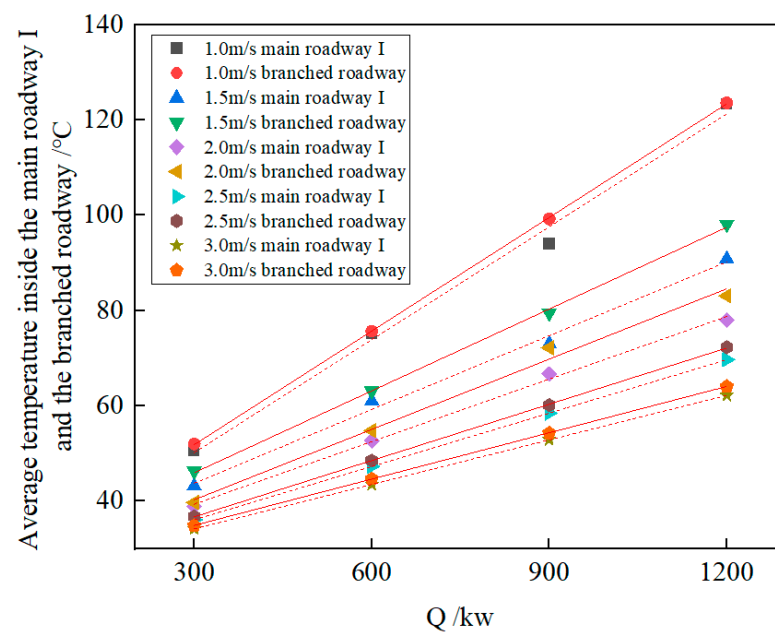


**Figure 8.** The variation in average temperature according to heat release rate.

The fitting lines are shown with solid lines and dashed lines in Figure 8. The values of  $c$  and  $d$  are displayed in Table 4. It can be seen from Figure 8 and Table 4 the values of R-squares are all above 0.99, which indicates that the variation in average temperature in the main roadway I and branched roadway according to heat release rate can be accurately predicted by Equation (6).

**Table 4.** The values of coefficients  $c$  and  $d$ .

The Type of Roadway	Ventilation Velocity/( $\text{m}\cdot\text{s}^{-1}$ )	$c$	$d$	$R^2$
The main roadway I	1.0	26.5	0.079	0.99343
	1.5	28.3	0.052	0.99442
	2.0	26.25	0.044	0.9977
	2.5	24.9	0.037	1
	3.0	24.85	0.031	1
The branched roadway	1.0	28.043	0.079	0.99994
	1.5	28.81	0.057	0.99919
	2.0	25.555	0.049	0.99254
	2.5	24.92	0.039	0.99991
	3.0	25.205	0.032	0.99999

### 3.3. The Profile of CO Concentration in the Main and Branched Roadway

Figure 9 presents the smoke propagation in the T-shaped roadway when the HRR is 600 kw and longitudinal ventilation velocity is 1.5 m/s. According to Figure 9, it can be seen that a high concentration of CO mainly gathers near the top plate of the fire source and spreads upstream of the fire source at a certain distance. Under the influence of longitudinal ventilation, the CO generated by the fire gradually spreads downstream of the main roadway and inside the branched roadway and then is rapidly diluted. The CO concentration in the main roadway I and branched roadway are much lower than near the fire source.

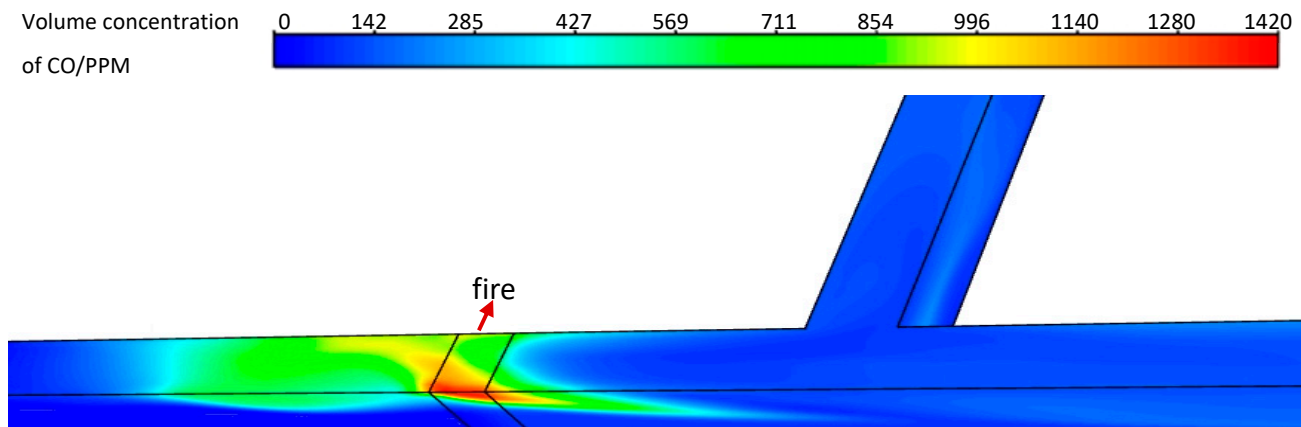


**Figure 9.** The volume concentration of CO in the T-shaped roadway (600 kw and 1.5 m/s).

Based on previous fire accident analyses, we know that high-temperature smoke contains CO, and casualties were partly caused by inhaling CO, so the distribution of CO concentration at breathing zone height is thoroughly analyzed and discussed in this section. Figure 10 shows the concentration distribution of CO at breathing zone height in the main roadway I and branched roadway under different longitudinal ventilation velocities when the HRR is 600 kw.

We can see clearly from Figure 10 that the concentration of CO at the height of the breathing zone in the main roadway I and branched roadway gradually decreases and tends to be of uniform distribution as the longitudinal ventilation velocity increases. When the ventilation velocities are 1 m/s and 1.5 m/s, the concentration of CO at the height of the breathing zone in the main roadway I is higher than in the branched roadway. And, when the ventilation velocities are 2 m/s, 2.5 m/s, and 3 m/s, respectively, the concentration of CO in the branched roadway is slightly higher than in the main roadway I.

The CO volume concentration in the safe evacuation passage is less than 500 ppm in the fire environment [28], so 500 ppm is chosen to be the critical concentration to escape safely for a person. The average concentration of CO at the breathing zone height inside the main roadway I and branched roadway is shown in Figure 11.

According to Figure 11, it can be seen that the average concentrations of CO in the main roadway I and branched roadway are all lower than 500 PPM. When the HRR is 900 kw, the maximum concentration difference between the main roadway I and branched roadway is 84.444PPM and the minimum concentration difference is 5.676 PPM. When the HRR is 600 kw, the maximum concentration difference is 19.72 PPM and the minimum concentration difference is 4.776 PPM. When the HRR is 300 kw, the maximum concentration difference is 54.094 PPM and the minimum concentration difference is 2.686 PPM. In addition, the concentration differences of CO between the main roadway I and the branched roadway decrease as the ventilation velocity increases. And we also can find that the average concentrations of CO inside the main roadway I and branched roadway decrease constantly with the increase in longitudinal ventilation velocity, which fits the power function. The fitting curves are shown in Figure 11 and the fitting functions are

shown in Table 5. The values of R-squares are all above 0.95 according to Figure 10 and Table 5; the equations describing the variation in average concentration of CO are shown in Table 5.

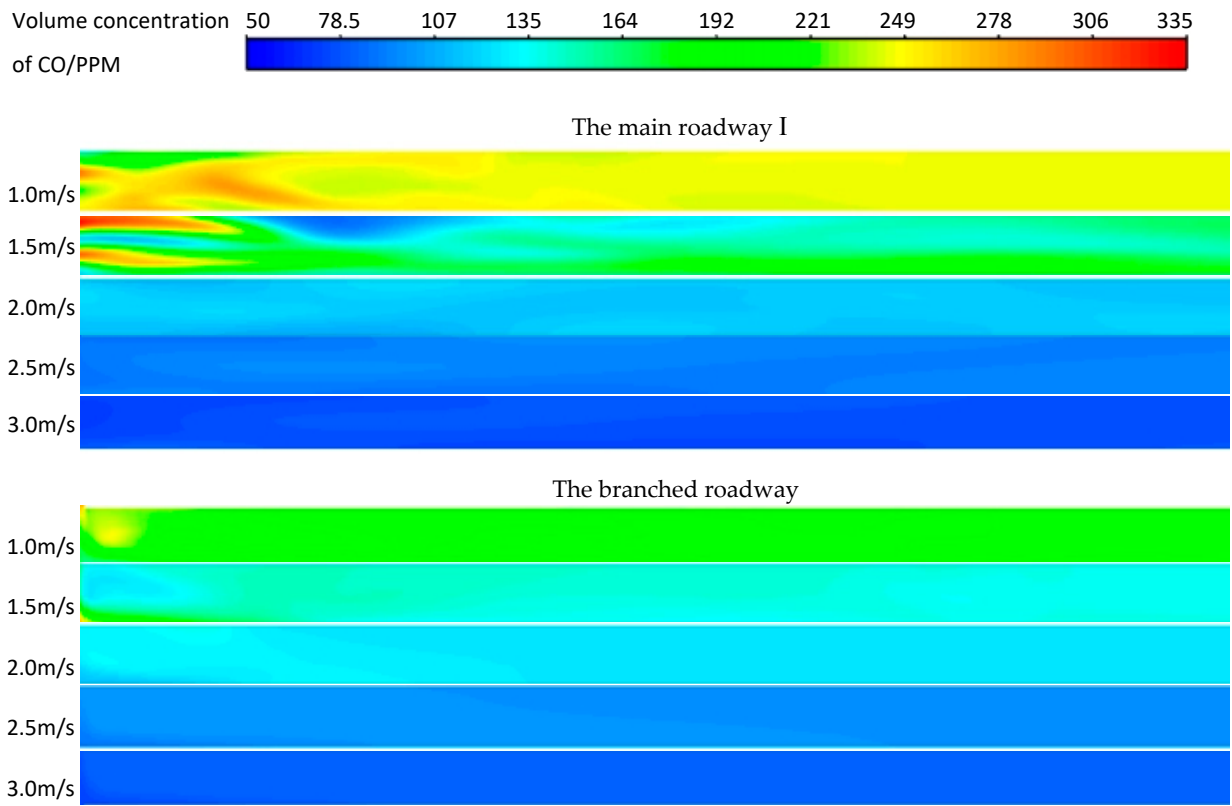


**Figure 10.** The concentration distribution of CO at breathing zone height in the T-shaped roadway (600 kw).

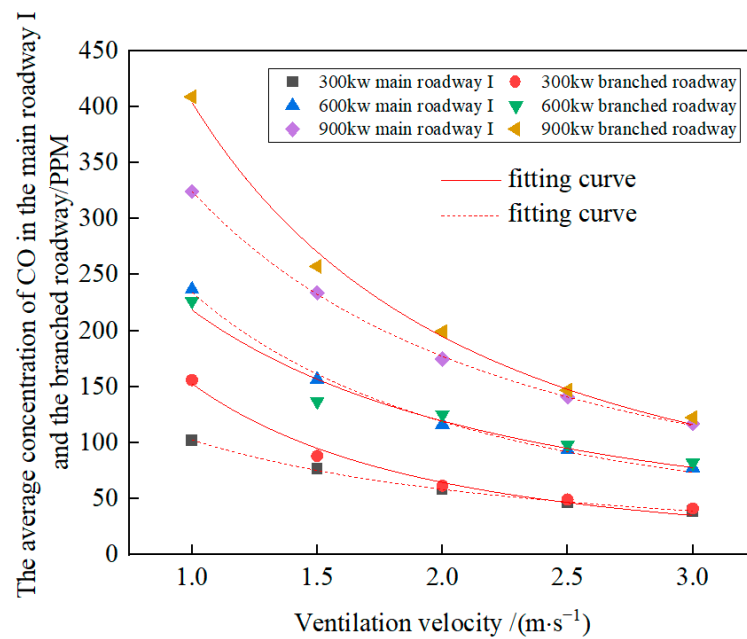


**Figure 11.** The average concentration of CO ( $Z = 1.6$  m) inside the main roadway I and branched roadway.

**Table 5.** The correlation equations between the average concentration of CO and longitudinal ventilation velocity.

The Type of Roadway	HRR/kw	Equation	R <sup>2</sup>
The main roadway I	300	$C = 269.693(1 + v)^{-1.39483}$	0.99855
	600	$C = 747.738(1 + v)^{-1.67461}$	0.99666
	900	$C = 913.481(1 + v)^{-1.49318}$	0.99963
The branched roadway	300	$C = 666.969(1 + v)^{-2.12719}$	0.98718
	600	$C = 613.838(1 + v)^{-1.49064}$	0.95877
	900	$C = 1404.458(1 + v)^{-1.79827}$	0.99514

C is the average concentration of CO at the breathing zone height (PPM).

The effect of HRR on average concentration of CO inside the main roadway I and the branched roadway are discussed then. Figure 12 shows the variation in the average concentration of CO according to the heat release rate. It can be seen that, as the heat release rate increases, the average concentration of CO inside the main roadway I and branched roadway increase linearly. And it can be described by the linear function; the fitting lines are shown in Figure 12 and the equations are presented in Table 6.

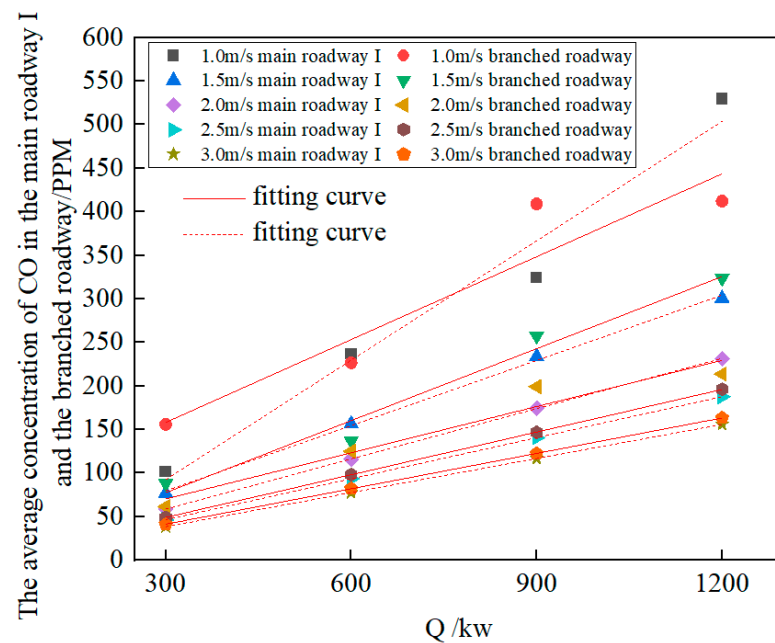


**Figure 12.** The variation in the average concentration of CO (Z = 1.6 m) according to heat release rate.

**Table 6.** The correlation equations between the average concentration of CO and heat release rate.

The Type of Roadway	Ventilation Velocity/(m·s <sup>-1</sup> )	Equation	R <sup>2</sup>
The main roadway I	1	$C = -44.6 + 0.457Q$	0.97318
	1.5	$C = 4.677 + 0.250Q$	0.99836
	2	$C = 0.870 + 0.192Q$	0.99997
	2.5	$C = -0.709 + 0.157Q$	1
	3	$C = -0.806 + 0.131Q$	1
The branched roadway	1	$C = 63.033 + 0.317Q$	0.89406
	1.5	$C = -5.233 + 0.276Q$	0.97509
	2	$C = 17.161 + 0.177Q$	0.94341
	2.5	$C = 0.154 + 0.163Q$	0.99999
	3	$C = 0.568 + 0.136Q$	0.99999

C is the average concentration of CO at the breathing zone height (PPM).

Table 6 illustrates that the value of R-squares is 0.89406 when the ventilation velocity is 1 m/s and the type of roadway is branched roadway. However, the values of R-squares are all above 0.94 in other cases. It can be explained that, when the ventilation velocity is 1 m/s, the volume of fresh airflow pushed into the branched roadway is much lower than in the main roadway I, so the mixing of smoke and fresh airflow is uneven, which leads to the disordered distribution of smoke in the branched roadway. Therefore, it can be concluded that the average concentration of CO inside the main roadway I and branched roadway can be predicted better by this kind of equation.

#### 4. Conclusions

In this paper, the influence of heat release rate and longitudinal ventilation velocity on smoke distribution in the bifurcated roadway is investigated by numerical simulation. The back-layering length, critical ventilation velocity, smoke temperature, and CO concentration at breathing zone height are analyzed and discussed. The conclusions are as follows:

- (1) The relationship between back-layering length and ventilation velocity under the same heat release rate is similar to a linear function in the T-shaped roadway. The ventilation velocity is the key factor influencing back-layering length, but the influence of heat release rate on back-layering length is gradually weakened when the HRR is above 600 kw.
- (2) By comparing the simulation data and the predicted model proposed by Wu [12] and Li [13], the critical ventilation velocity in the T-shaped roadway is higher than in a single-tube roadway when the fire source locates upstream of the T-junction. A prediction model of dimensional critical ventilation velocity in the T-shaped bifurcated roadway is proposed, which also fits a power function of  $1/3$ .
- (3) The temperatures in the main roadway I and branched roadway are conducive to escape when the HRR is 300 kw and the ventilation velocity is between 1 m/s and 3 m/s, when the HRR is 600 kw and the ventilation velocity is in the range from 2 m/s to 3 m/s, and when the HRR is 900 kw and the ventilation velocities are 2.5 m/s and 3 m/s, respectively. The correlation between average temperature ( $Z = 1.6$  m) in the main roadway I and branched roadway and ventilation velocity fits the power function. And the variation in average temperature ( $Z = 1.6$  m) according to HRR fits the linear function.
- (4) The workers in the main roadway I and branched roadway are less susceptible to fire smoke and toxic gases when the HRRs are 300 kw and 600 kw and the ventilation is between 1 m/s and 3 m/s. The relationship between average concentration of CO ( $Z = 1.6$  m) inside the main roadway I and branched roadway and longitudinal ventilation velocity follows the power formula. And the variation in average concentration of CO ( $Z = 1.6$  m) according to the HRR follows the linear function trend.

**Author Contributions:** C.D.: Conceptualization, Formal analysis, Supervision. D.C.: Methodology, Investigation. D.S.: Software, Writing (original draft). S.Z.: Software. All authors have read and agreed to the published version of the manuscript.

**Funding:** This research was funded by the State Key Laboratory Cultivation Base for Gas Geology and Gas Control (Henan Polytechnic University), grant number "WS2022B11".

**Institutional Review Board Statement:** Not applicable.

**Informed Consent Statement:** Not applicable.

**Data Availability Statement:** Data are contained within the article.

**Conflicts of Interest:** The authors declare no conflicts of interest.

## References

1. Liu, Y.J.; Xue, J.H.; Yuan, L.; Tian, Z.C.; Deng, D.S. Simulation analysis of variation law of smoke flow parameters during tunnel being on fire. *China Min. Mag.* **2018**, *27*, 144–150.
2. Tian, S.C.; Dou, P.Q.; Zhang, C.Z. Impact of Different Wind Speeds on the Law of Mine Fire Spread Based on Pyrosim. *Met. Mine* **2020**, *44*, 199–204.
3. Jia, J.; Guo, L.W.; Zhu, L.Q.; Zhang, J.Y. Study on numerical simulation of smoke backflow and critical wind speed in mine roadway fire. *J. Saf. Sci. Technol.* **2020**, *16*, 94–100.
4. Shen, Y.G.; Wang, D.M. Numerical Simulation of Smoke Disaster Caused by Mine Roadway Fire Based on FDS. *Saf. Coal Mines* **2020**, *51*, 183–187.
5. Xue, Y.P. Numerical Simulation of Effect of Tunnel Diverging Angles on Fire Smoke Flow. *Saf. Coal Mines* **2020**, *51*, 179–183.
6. Lu, G.L.; Tian, M.Y. Study on the fire smoke flow characteristics in T-type roadway of deep well. *Min. R D* **2020**, *40*, 106–111.
7. Gao, Y.J.; Luo, Y.Y.; Li, Z.S.; Zhang, Y.C.; Yu, Y.Y.; Li, T. Experimental study on smoke back-layering length and temperature distribution in bifurcation tunnels. *China Saf. Sci. J.* **2022**, *32*, 109–115.
8. Huang, Y.; Li, Y.; Li, J.; Li, J.; Wu, K.; Zhu, K.; Li, H. Experimental investigation on maximum gas temperature beneath the ceiling in a branched tunnel fire. *Int. J. Therm. Sci.* **2019**, *145*, 105997. [[CrossRef](#)]
9. Huang, Y.B.; Li, Y.F.; Li, J.X.; Wu, K.; Li, H.H.; Zhu, K.; Li, J.M. Experimental investigation of the thermal back-layering length in a branched tunnel fire under longitudinal ventilation. *Int. J. Therm. Sci.* **2022**, *173*, 107415. [[CrossRef](#)]
10. Chen, C.K.; Jiao, W.B.; Zhang, Y.L.; Peng, L. A comparative study on smoke temperature profile and corresponding different-exponential form correlation in single-line and bifurcated tunnel fires. *Tunn. Undergr. Space Technol.* **2023**, *136*, 105090. [[CrossRef](#)]
11. Tao, L.L.; Zeng, Y.H.; Yang, G.C.; Zhao, D.X.; Li, J.; Fu, X.K. Ceiling temperature distribution and decay in tunnel fires: Effect of longitudinal velocity, bifurcated shaft exhaust and fire location. *Case Stud. Therm. Eng.* **2023**, *41*, 102651. [[CrossRef](#)]
12. Wu, Y.; Bakar, M.Z.A. Control of smoke flow in tunnel fires using longitudinal ventilation systems—A study of the critical velocity. *Fire Saf. J.* **2000**, *35*, 363–390. [[CrossRef](#)]
13. Li, Y.Z.; Lei, B.; Ingason, H. Study of critical velocity and backlayering length in longitudinally ventilated tunnel fires. *Fire Saf. J.* **2010**, *45*, 361–370. [[CrossRef](#)]
14. Zhang, T.H.; Wang, G.Y.; Li, J.D.; Huang, Y.D.; Zhu, K.; Wu, K. Experimental study of back-layering length and critical velocity in longitudinally ventilated tunnel fire with various rectangular cross-sections. *Fire Saf. J.* **2021**, *126*, 103483. [[CrossRef](#)]
15. Lee, S.R.; Ryou, H.S. An Experimental Study of the Effect of the Aspect Ratio on the Critical Velocity in Longitudinal Ventilation Tunnel Fires. *J. Fire Sci.* **2005**, *23*, 119–138. [[CrossRef](#)]
16. Minehiro, T.; Fujita, K.; Kawabata, N.; Hasegawa, M.; Tanaka, F. Backlayering distance of thermal fumes in tunnel fire experiments using a large-scale model. *J. Fluid Sci. Technol.* **2012**, *7*, 389–404. [[CrossRef](#)]
17. Ingason, H.; Li, Y.Z. Model scale tunnel fire tests with longitudinal ventilation. *Fire Saf. J.* **2010**, *45*, 371–384. [[CrossRef](#)]
18. Tsai, K.C.; Lee, Y.P.; Lee, S.K. Critical ventilation velocity for tunnel fires occurring near tunnel exits. *Fire Saf. J.* **2011**, *46*, 556–557. [[CrossRef](#)]
19. Tanaka, F.; Takezawa, K.; Hashimoto, Y.; Moinuddin, K.A. Critical velocity and backlayering distance in tunnel fires with longitudinal ventilation taking thermal properties of wall materials into consideration. *Tunn. Undergr. Space Technol.* **2018**, *75*, 36–42. [[CrossRef](#)]
20. Gannouni, S.; Maad, R.B. Numerical study of the effect of blockage on critical velocity and backlayering length in longitudinally ventilated tunnel fires. *Tunn. Undergr. Space Technol.* **2015**, *48*, 147–155. [[CrossRef](#)]
21. Gannouni, S.; Maad, R.B. CFD analysis of smoke backlayering dispersion in tunnel fires with longitudinal ventilation. *Fire Mater.* **2017**, *41*, 598–613. [[CrossRef](#)]
22. Lu, X.L.; Weng, M.C.; Liu, F.; Wang, F.; Han, J.Q.; Cheung, S.C. Effect of bifurcation angle and fire location on smoke temperature profile in longitudinal ventilated bifurcated tunnel fires. *Tunn. Undergr. Space Technol.* **2022**, *127*, 104610. [[CrossRef](#)]
23. Liu, F.; Han, J.Q.; Wang, F.; Wang, Z.H.; Weng, M.C. Experimental study on the temperature profiles in a naturally ventilated metro tunnel with a transverse cross-passage. *Tunn. Undergr. Space Technol.* **2021**, *116*, 104094. [[CrossRef](#)]
24. Ding, C.; He, X.Q.; Nie, B.S. Numerical simulation of airflow distribution in mine tunnels. *Int. J. Min. Sci. Technol.* **2017**, *27*, 663–667. [[CrossRef](#)]
25. Ding, C. Study on distribution characteristics of “characteristic ring” and “key ring” in mine ventilation roadway during fires. *J. Saf. Sci. Technol.* **2017**, *13*, 55–60.
26. He, X.Q. *Theory and Technology for the Prevention of Coal Mine Disasters*; China University of Mining and Technology Press: Xuzhou, China, 2006; pp. 276–278.
27. Ding, C. Numerical research on fire smoke distribution in highway tunnels. *Ind. Saf. Environ. Prot.* **2022**, *48*, 5–8+44.
28. Sun, L.Q. *The Study on Smoke Spread and Main Influencing Factors in Typical Mine Tunnel Exogenous Fire*; Taiyuan University of Technology: Taiyuan, China, 2018.

**Disclaimer/Publisher’s Note:** The statements, opinions and data contained in all publications are solely those of the individual author(s) and contributor(s) and not of MDPI and/or the editor(s). MDPI and/or the editor(s) disclaim responsibility for any injury to people or property resulting from any ideas, methods, instructions or products referred to in the content.